POLITECNICO DI TORINO
Repository ISTITUZIONALE

Temperatures evaluation in an integrated motor drive for traction applications

Original
Temperatures evaluation in an integrated motor drive for traction applications / Tenconi, Alberto; Profumo, Francesco; S. E., Bauer; M. D., Hennen. - In: IEEE TRANSACTIONS ON INDUSTRIAL ELECTRONICS. - ISSN 0278-0046. - STAMPA. - 55:10(2008), pp. 3619-3626. [10.1109/TIE.2008.2003099]

Availability:
This version is available at: 11583/1855997.5 since:

Publisher:
IEEE

Published
DOI:10.1109/TIE.2008.2003099

Terms of use:
openAccess

This article is made available under terms and conditions as specified in the corresponding bibliographic description in the repository

Publisher copyright

(Article begins on next page)

05 May 2023

Temperatures Evaluation in an Integrated Motor Drive for Traction Applications

Alberto Tenconi, *Member, IEEE*, Francesco Profumo, *Senior Member, IEEE*, Stefan E. Bauer, and Martin D. Hennen, *Member, IEEE*

***Abstract*—The integrated propulsion motor is a drive designed for an individual self-driven container rail-platform wagon developed in the "Integrated Standard Transport Unit" research and development project, supported by the European Commission. This paper presents the study of the motor and the converter temperatures at rated and overload working conditions. The problem is afforded by combining the simulation (finite-element method and lumped-parameter models) and the experimental approaches. For this purpose, a dedicated experimental setup has been designed and realized.**

***Index Terms*—Integrated motor drives, motor-drive thermal factors, switched reluctance motor (SRM) drives.**

I. Introduction

THIS PAPER deals with the liquid-cooled totally integrated drive unit Integrated Propulsion MOTor (IPMOT) shown in Fig. 1. The IPMOT has been developed for an individual self-driven rail-platform wagon for freight container transport within closed areas (seaports, cargo distribution centers, etc.); the overall reliability demand of this autonomous operating vehicle has been satisfied by redundancy, employing two independent IPMOT units on each wagon, supplied by a single diesel-electric group. The low speed and the low acceleration of the vehicle bring to 24-kW power rating for each motor, with a 1:5 constant power speed range [1]: These specifications make the drive performances comparable with those required by electric- and hybrid-vehicle applications [2]–[4].

The propulsion motor is a four-phase switched reluctance motor (SRM) [1]. The choice of SRM is justified by its inherent reliability and the low-cost technology [5]–[8]. The motor is fed by eight insulated-gate bipolar-transistor (IGBT)-based hard-switching [9] digital-controlled [10] power electronic converter.

It is expected that the integration of the motor with the power electronic converter brings more reliability, size reduction, and economic advantages with respect to the conventional separated solution [11]–[13].

Manuscript received December 23, 2007; revised July 22, 2008. Current version published October 1, 2008. This paper is part of the Integrated Standard Transport Unit (ISTU) Research and Development Project (STREP) and was supported by the European Commission.

A. Tenconi and F. Profumo are with the Dipartimento di Ingegneria Elettrica, Politecnico di Torino, 10129 Turin, Italy (e-mail: alberto.tenconi@polito.it).

S. E. Bauer is with Durotron, 51109 Cologne, Germany (e-mail: bauer@durotron.de).

M. D. Hennen is with the Institute for Power Electronics and Electrical Drives, RWTH Aachen University, 52066 Aachen, Germany (e-mail: martin.mennen@isea.rwth-aachen.de).

Color versions of one or more of the figures in this paper are available online at http://ieeexplore.ieee.org.

Digital Object Identifier 10.1109/TIE.2008.2003099

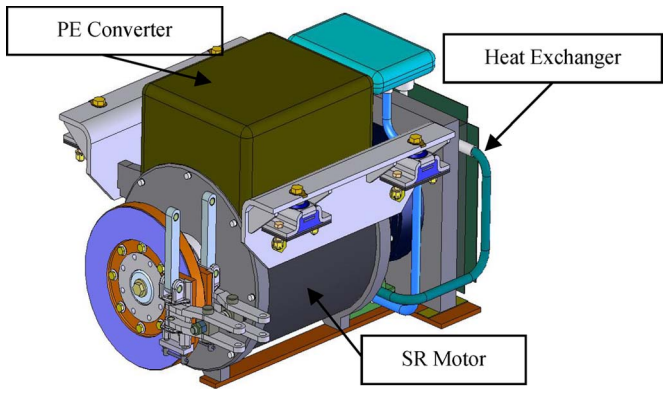

Fig. 1. IPMOT unit.

Currently, most of the integrated motors available on the market are focused on low-power applications and consist of a machine and a converter separately conceived and then assembled together to obtain a single device. This solution gets rid of cables and solves some electromagnetic-interference problems, but it does not exploit completely the potential benefits in terms of space and weight reduction, particularly interesting in the transport applications [14].

For a complete thermal–mechanical integration, the motor housing must act as heatsink for the power electronic converter [15]–[17]. For liquid-cooled drives, one of the most compact solution is based on a square-shaped housing, with cooling water pipes inserted in the corner; the square frame makes possible the electronic-component integration on the flat surface of the housing, as proposed in a preliminary study [8]. This solution presents cost and manufacturing problems in the optic of small/medium production volume. Hence, the solution shown in Fig. 2 has been chosen, where the motor and the converter can be realized and tested separately and, then, can be easily mounted together.

From the thermal point of view, this solution is a tradeoff between the one of [8] and the conventional ones: There is a single cooling circuit for both the motor and the converter, but the water jacket around the motor basically shields any direct heat exchange between the motor and the converter; i.e., the motor and the converter are mechanically integrated, but they are thermally coupled only trough the liquid cooling circuit.

This paper presents the study of the temperatures of the integrated drive, at rated and overload working conditions, using both finite-element-method (FEM) and lumped-parameter models. The SRM thermal modeling is synthetically summarized (the magnetic and thermal design is presented in details

0278-0046/$25.00 © 2008 IEEE

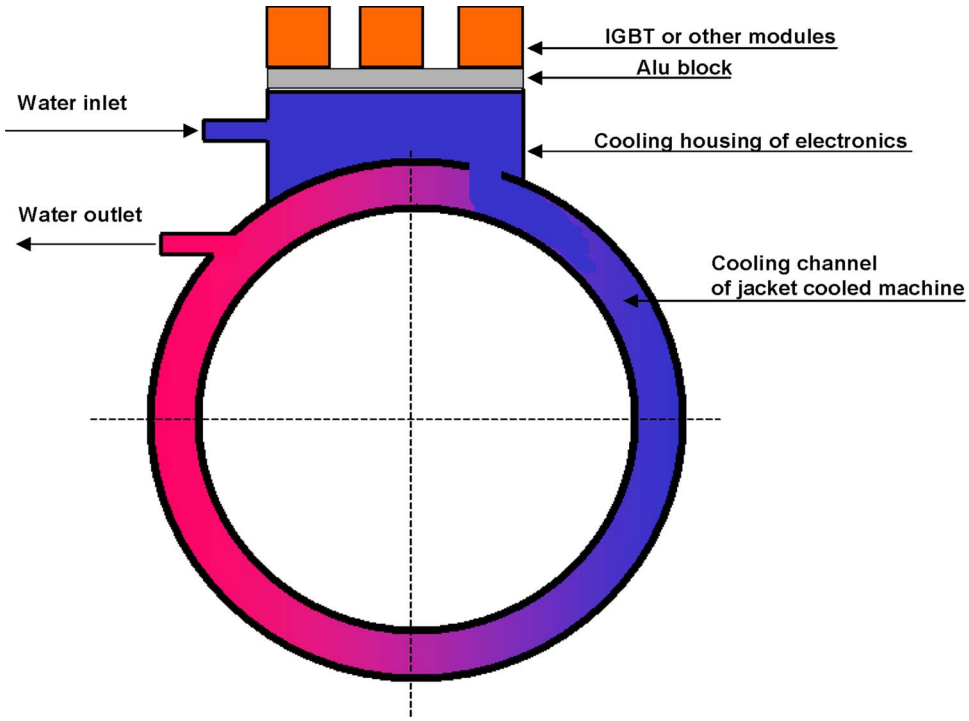

Fig. 2. Scheme of the thermal integration of the motor and the converter.

in [8]) and compared with some experimental results; the main focus is devoted to the thermal contact between the motor housing and the base plate supporting the power-electronic components of the power converter. In particular, the thermal evaluations are tuned by means of experimental measurements.

II. Problem Description

In the IPMOT, the motor is cooled by a water jacket all around the stator. The rotor losses in SRMs are estimated to be in the range of half of the core losses [18], [19]. In the case under study, the rotor losses are estimated to be no more than 10% of the total motor losses.

For this reason, the focus of this paper is basically concentrated on the stator-winding temperatures; in particular, the key point is the evaluation of the heat-exchange coefficients due to the insulation materials and the contact surfaces between windings and iron [20], [21]. In the IPMOT, the water pipes are obtained in the motor housing (made of steel), and the power modules are mounted on an aluminum base plate that is fixed on the upper side of the motor housing. This layout (Fig. 3) has one more layer as compared to the common heatsinks, where the water pipes are directly worked in the cold plate. For this reason, a dedicated investigation is required to evaluate the IPMOT thermal behavior; in particular, it is necessary to evaluate the effect of the contact surface between the motor housing and the aluminum base plate on the junction temperature of the power components.

The contact area of two plane surfaces generates a thermal contact resistance; the heat-exchange coefficient depends on the flatness and the roughness of these surfaces. In principle, knowing the physical parameters of the two surfaces, it is possible to estimate the thermal contact resistance; in practice, the pressure between the two surfaces plays an important role, and

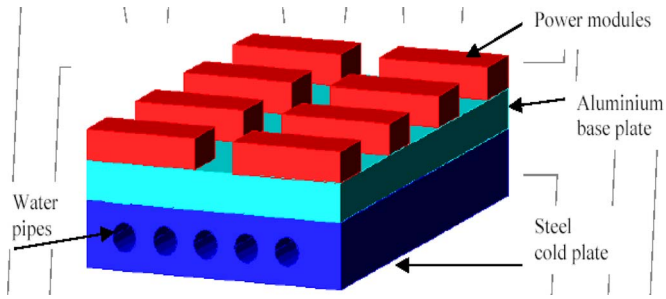

Fig. 3. Simplified layout of the heatsink system of the IPMOT.

some experimental tests are necessary in tuning the parameters of the thermal model of the power-electronic part. Once the thermal circuit is experimentally tuned, it can be used for the temperature evaluations of the critical point of the system, i.e., the junction temperature of the power-electronic components, that must stay below 125 °C−150 °C.

III. Motor Temperatures

A. FEM Approach on the Motor

In the IPM1OT prototype, the water jacket is manufactured from a metal sheet with rectangular section. Since the power-electronic components are mounted on a separated cooling housing, the FEM simulations (Fig. 4) have been performed considering only the motor losses. The temperature has been assumed constant along the external stator surface, and the copper losses has been supposed equally distributed over the conductors section; a total power dissipation of 2.5 kW has been considered.

SRMs have concentrated windings, and the coils are mounted on the stator teeth; this solution leaves an empty triangular area between two adjacent coils, thus reducing the surface available

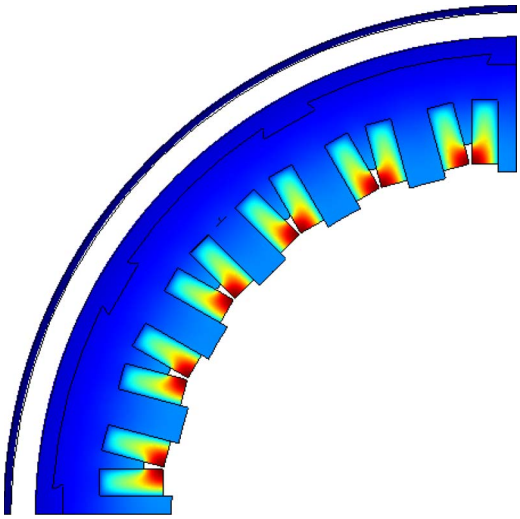

Fig. 4. Temperature distribution on the SRM with water-jacket cooling.

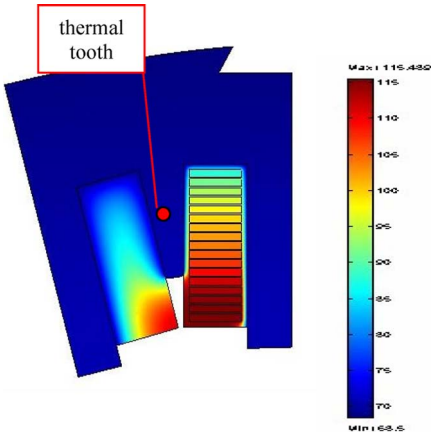

Fig. 5. Comparison between real and equivalent winding models.

for the thermal contact between copper and iron. Furthermore, to reduce the additional copper losses (eddy currents, skin effect) [22], [23], the conductors are disposed parallel to the slot base, that leads to a higher thermal resistance along the radial direction. Since the copper–iron thermal resistance is the largest one in the thermal equivalent circuit of the machine, the reduction of the temperature gradient between copper and iron significantly reduces the total temperature gradient between the copper and the cooling fluid. For this reason, an auxiliary "thermal tooth" (Fig. 5) made of iron has been inserted to fill the triangle area: The iron triangles increase the thermal contact surface, improving the heat transmission through the coils sides, with only a little influence in torque production, if the height of a thermal triangle is sufficiently small [1].

In simulating, the thermal behavior of the motor, to avoid too heavy mesh refinement during finite-element analysis, the standard winding (constituted by copper straps and insulation), has been substituted by a homogeneous material with the anisotropic thermal proprieties, emulating the temperatures on the copper–iron contact surface (Fig. 5). This simulation approach is discussed and validated in [8]. In the next section, the experimental results confirm the temperature evaluations given by the FEM model.

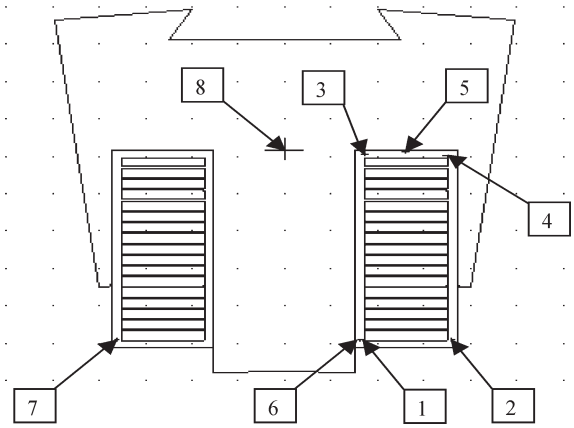

Fig. 6. Location of the thermocouples inside the motor.

TABLE I
COMPARISON BETWEEN SIMULATED AND MEASURED MOTOR TEMPERATURES AT THE NOMINAL LOAD (INLET = 60 °C, INLET—OUTLET GRADIENT= 5 °C)

Sensors	$\vartheta_{MEASURE}$ [°C]	ϑ_{SIMU}[°C]	$\Delta\vartheta$ [°C]
1	109	109	0
2	114	115	1
3	79	79	0
4	84	83	0
5	75	75	0
6	94	94	0
7	108	115	7
8	75	72	-3

B. Experimental Results

For accurate measurements, the motor have been equipped with eight thermal sensors (Fig. 6) and loaded by means of a test bench. Considering the iron and copper losses in the nominal working point, the simulated and measured temperatures are reported in Table I (the motor-drive ratings are reported in the Appendix).

Except $\vartheta_{\text{sensor\_7}}$, the differences between the simulated and the measured temperatures are not significant, and the experimental results validate the finite-element model. The difference between the values measured by sensor_7 and the symmetrical sensor_2 is due to the different eddy-current losses distribution in the copper straps, depending on the rotation direction; this effect is not considered in the simulation, and it explains the difference between the measured and simulated values of $\vartheta_{\text{sensor\_7}}$.

IV. POWER-ELECTRONIC TEMPERATURES

The power-electronic components of the integrated motor drive are mounted on an aluminum base plate that is fixed on the upper side of the motor housing. The temperatures of the IGBT and diode junctions can be quickly computed using a lumped-parameter steady-state thermal model [24], [25]. The key problem is the correct determination of the thermal-resistance values: The values concerning the power-electronic components are available from the data sheet; the values concerning the heatsink system must be computed. Some uncertainties arise from the contact surface between the motor housing and

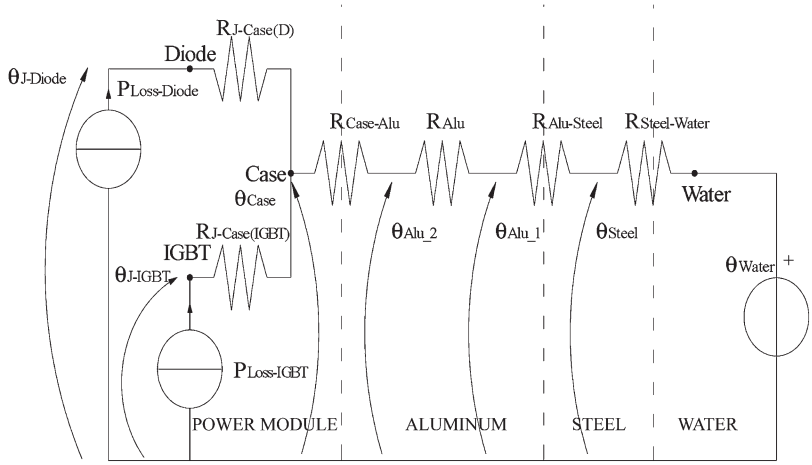

Fig. 7. Electric equivalent of the thermal circuit of a single-power-module cooling system.

the aluminum base plate. Since the effect of some physical parameters of the contact surface are not perfectly known (the pressure between the surfaces, in particular), some experimental tests are necessary in tuning the thermal evaluations.

A. Thermal Model

The lumped-parameter steady-state thermal model of a single power module (one IGBT and one diode in the same case) mounted on the liquid cooling heatsink is shown in Fig. 7. The inputs of the model are the losses in the power module ($P_{\mathrm{Loss-Diode}}$ and $P_{\mathrm{Loss-IGBT}}$) and the water temperature ($\vartheta_{\mathrm{Water}}$). The outputs of the model are the temperatures of the junctions ($\vartheta_{\mathrm{J-Diode}}$ and $\vartheta_{\mathrm{J-IGBT}}$). In the model, there are six thermal resistances to be determined:

$R_{\mathbf{J-Case(IGBT)}}$	due to the internal structure of the module;
$R_{\mathbf{J-Case(Diode)}}$	due to the internal structure of the module;
$R_{\mathbf{Case-Alu}}$	due to the contact between the upper face of the aluminum base plate and the case of the module;
$R_{\mathbf{Alu}}$	due to the thickness of the aluminum base plate;
$R_{\mathbf{Alu-Steel}}$	due to the contact between the steel and aluminum surfaces;
$R_{\mathbf{Steel-Water}}$	constituted by the following two terms: the first one is due to the steel thickness of the housing and the second one is due to the contact between the water and the walls of the pipes.

The first three thermal resistances are given in the data sheet of the components.

The last three thermal resistances must be computed on the basis of the geometries and of the thermal conductivity of the materials and, then, tuned by means of experimental measurements. For this purpose, a dedicated experimental setup has been developed to emulate the thermal integration between the converter heatsink and the motor housing; for the sake of completeness, the experimental setup has been also simulated by a FEM tool.

1) Experimental Setup: The experimental setup (Fig. 8) is made of an aluminum plate fixed on a steel plate where the cooling water flows through three circular pipes connected in series; on the aluminum base plate, four electric resistors are fixed, emulating the power losses of the electronic modules. The aluminum plate is fixed by screws: The number of screws can be adjusted to test different mechanical couplings.

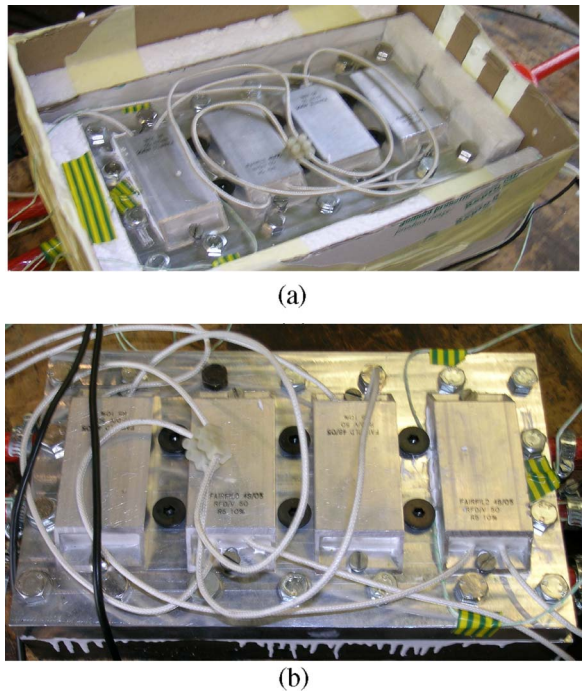

(a)

(b)

Fig. 8. Experimental setup (a) with and (b) without thermal insulation.

To have meaningful results, the qualities of the two surfaces are in the range of conventional machining:

steel flatness	12 μm;
steel roughness	1.4 μm;
aluminum flatness	72 μm;
aluminum roughness	0.8 μm.

For practical reasons, the experimental setup reproduces approximately one half of the real situation (four power modules instead of eight). In order to have similar paths of the heat fluxes and similar temperature distribution near the component case, the dimensions of the resistors are quite closed to the

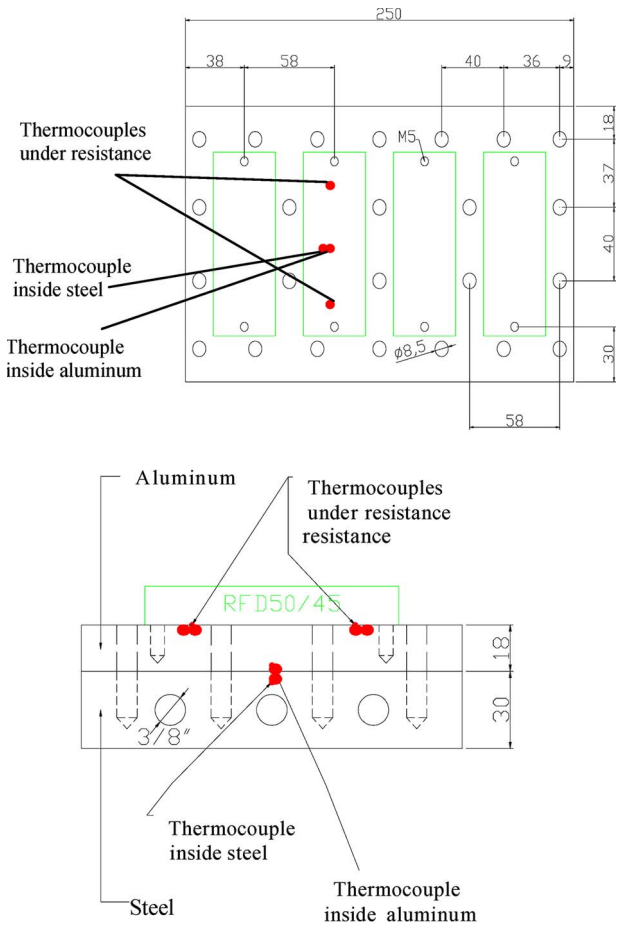

Fig. 9. Experimental setup geometry and position of thermocouples.

dimensions of the IPMOT's power-electronic modules. The resistors can dissipate up to 100 W; therefore, it is possible to reach the losses level of the IPMOT's electronic components.

Since the overall system is thermally insulated, to limit the convective thermal exchange with ambient air, the largest part of the electric input power is dissipated through the aluminum base plate to the water.

The temperatures are measured by six thermocouples laid out as shown in Fig. 9:

- one thermocouple inside the steel plate $\vartheta_{\mathrm{Steel}}$;
- one thermocouple in the aluminum base plate $\vartheta_{\mathrm{Alu\_1}}$;
- four thermocouples under the resistor, $\vartheta_{\mathrm{UR}} \approx \vartheta_{\mathrm{Alu\_2}}$.

ϑ_{UR} is the temperature measured under the resistors in the contact area between the upper face of the aluminum base plate and the case of the dissipating resistors. ϑ_{UR} can be considered quite close to $\vartheta_{\mathrm{Alu\_2}}$ (Fig. 7). To have the proper thermal contact in this area, the surfaces of the resistors and the sensors have been covered by a commercial thermal-joint compound of thermally loaded silicon-based grease [thermal conductivity of 0.39 $\mathrm{W}/(\mathrm{m}\cdot\mathrm{K})$].

2) Experimental Results: Two sets of experimental tests have been performed to evaluate separately the effect of the mechanical coupling and the effect of the thermal-joint compound on the thermal resistance due to the contact surface between the aluminum base plate and the steel motor housing. In the first set, the surfaces are without thermal-joint compound; in the second one, the surfaces are covered by thermal-joint compound.

TABLE II
TEST WITHOUT THERMAL-JOINT COMPOUND BETWEEN THE ALUMINUM AND STEEL PLATES

Test	N° of screws	$\vartheta_{\mathrm{Steel}}$ °C	ϑ_{Alu} °C	ϑ_{UR} °C	$\Delta\vartheta_{\mathrm{Alu\text{-}Steel}}$ °C	$\Delta\vartheta_{\mathrm{UR\text{-}Water}}$ °C
1	4	20	34	43	14	28
2	8	20	30	41	10	25
3	24	20	24	32	4	17

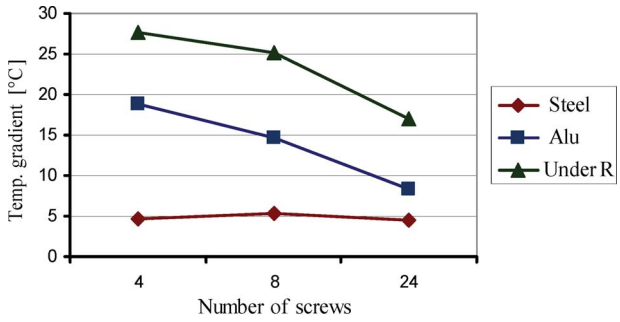

Fig. 10. Temperature gradient of the steel and aluminum plates and under the resistor respect to the water temperature—tests *without thermal-joint compound.*

Each set considers three tests with different number of screws fixing the two parts.

SET 1

TEST 1) 4 screws—without thermal-joint compound;
TEST 2) 8 screws—without thermal-joint compound;
TEST 3) 24 screws—without thermal-joint compound.

SET 2

TEST 4) 4 screws—with thermal-joint compound;
TEST 5) 8 screws—with thermal-joint compound;
TEST 6) 24 screws—with thermal-joint compound.

The working conditions in all the six tests are as follows:

ambient temperature	18 °C;
water temperature	15.5 °C;
water flow	10 $\mathrm{dm}^3/\mathrm{min}$;
total electric power	416 W (104 W per resistor).

SET 1—dry surfaces: Table II and Fig. 10 synthesize the experimental results with different number of screws when the aluminum and steel surfaces are without thermal-joint compound: The temperature gradient between aluminum and steel is strongly affected by the number of screws. Furthermore, TEST 1) shows that, in this case (few screws and dry surfaces), the temperature gradient on the steel–aluminum contact surface is rather large, significantly impacting on the temperature gradient $\Delta\vartheta_{\mathrm{UR-Water}}$.

SET 2—surfaces with thermal-joint compound: Table III synthesizes the experimental results with different number of screws when the aluminum and steel surfaces are covered by thermal-joint compound.

Table III shows how the temperature difference between aluminum and steel is not affected any more by the number of screws. These tests also show that, using the thermal-joint compound, the temperature gradients on the steel–aluminum contact surface is rather small; hence, it will have a limited

TABLE III
TEST WITH THERMAL-JOINT COMPOUND BETWEEN ALUMINUM AND STEEL

Test	N° of screws	ϑ_{Steel} °C	ϑ_{Alu} °C	ϑ_{UR} °C	$\Delta\vartheta_{Alu\text{-}Steel}$ °C	$\Delta\vartheta_{UR\text{-}Water}$ °C
4	4	21	24	32	3	17
5	8	21	24	32	3	17
6	24	21	23	32	2	16

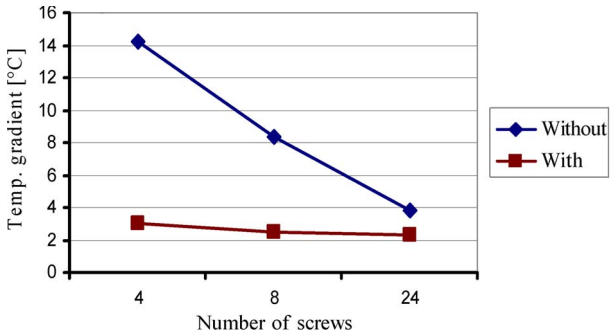

Fig. 11. Temperature gradients between aluminum and steel with and without thermal-joint compound.

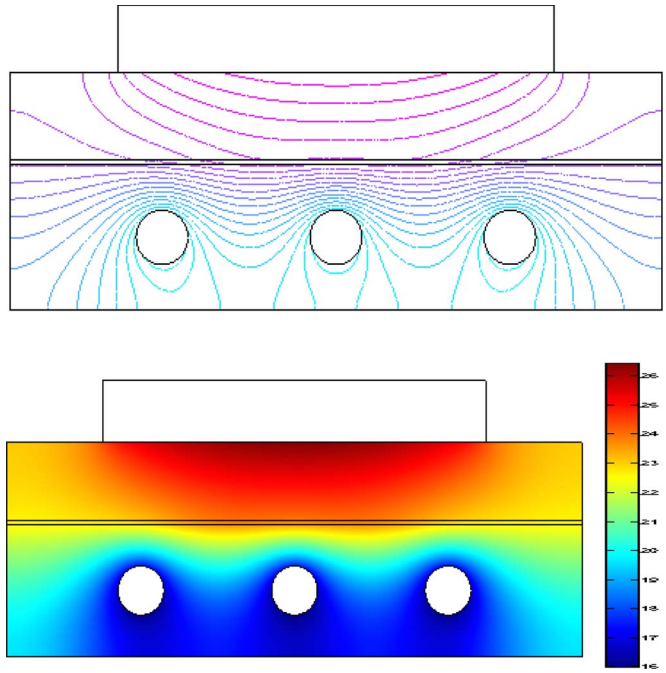

Fig. 12. FEM simulation of the experimental setup.

impact on the temperature gradient $\Delta\vartheta_{\mathrm{UR-Water}}$. Finally, Fig. 11 shows how the use of the thermal-joint compound almost cancels the effect of the number of screws on the temperature gradient between aluminum and steel.

In conclusion, the temperature gradient due to the steel–aluminum contact surface can have a limited impact on the temperature of the power modules (with respect to the cooling water), provided that the thermal-joint compound between the contact surfaces is adopted or the two surfaces are fixed by a sufficient number of screws.

3) FEM Results: For sake of completeness, the experimental setup has been also simulated, adopting FEM (Fig. 12). The basic assumptions are as follows.

1) The roughness of the wall of pipes is 300 μm (standard value for this material and type of tooling process). This value affects the convection coefficient between water and steel.
2) Due to the imperfect setup insulation from the ambient [Fig. 8(a)], even if the largest part (more than 90%) of the dissipated power reaches the water, it has been considered also a minor part dissipated by air natural convection.

The FEM model can simulate the steel–aluminum contact resistance and fits the experimental results, tuning the thickness of the air layer between the steel and the aluminum layer.

B. Junction-Temperature Evaluation

The main goal is the evaluation of the junction temperature of the power components ($\vartheta_{\mathrm{J-Diode}}$ and $\vartheta_{\mathrm{J-IGBT}}$) in the most severe working conditions. Since the heat-exchange path in the IPMOT and in the experimental setup are similar, the steady-state temperatures can be computed, adopting the values of the parameters of the thermal model in Fig. 7, tuned by the experimental tests.

The values of the thermal resistances are the following.

- $R_{\mathrm{Steel-Water}} = 0.055$ °C/W, from the experimental tests.
- $R_{\mathrm{Alu-Steel}} = 0.021$ °C/W, best solution, test 6 (Table III).
- $R'_{\mathrm{Alu-Steel}} = 0.15$ °C/W, worst solution, test 1 (Table II).
- $R_{\mathrm{Case-Alu}} = 0.050$ °C/W, from data sheet.
- $R_{\mathrm{J-Case-(IGBT)}} = 0.13$ °C/W, from data sheet.
- $R_{\mathrm{J-Case-(Diode)}} = 0.30$ °C/W, from data sheet.
- $R_{\mathrm{Alu}} = 0.023$ °C/W, from the FEM simulations and experimental tests. The value has been determined by two methods: The first one uses the average temperature computed by FEM simulations on the upper and lower faces of the aluminum plate, and the second one employs a standard formula but considering that the greatest part of the heat flux passes through only a reduced section (equal to the surface of the resistor base), instead of the total surface of the aluminum base plate. The two methods give similar results, also confirmed by the experimental tests.

1) Temperatures Evaluation at Rated Load: At rated load, the power losses in each module (diode + IGBT) are about 100 W; the junction temperature of the power components ($\vartheta_{\mathrm{J-Diode}}$ and $\vartheta_{\mathrm{J-IGBT}}$) can be evaluated by considering different working conditions (losses). In particular, three different sharing of the total losses between the diode and the IGBT in the same power module has been considered:

1) all the losses in the diode;
2) all the losses in the IGBT;
3) 2/3 of the power losses in IGBT and 1/3 in the diode.

The first two conditions are not realistic but have been considered as extreme situations; the third sharing ratio is representative of an average real situation.

In Table IV, the temperatures are calculated considering the worst mounting solution (four screws without thermal-joint compound), whereas Table V reports the temperatures for the best mounting solution (24 screws with thermal-joint compound).

TABLE IV
TEMPERATURE GRADIENTS AND JUNCTION TEMPERATURES AT $\vartheta_{Water} = 65$ °C (WORST SOLUTION—FOUR SCREWS WITHOUT THERMAL-JOINT COMPOUND)

Losses sharing	$P_{Loss\text{-}Diode}$	$P_{Loss\text{-}IGBT}$	$\Delta\vartheta_{Case\text{-}Water}$	$\Delta\vartheta_{Diode\text{-}Water}$	$\Delta\vartheta_{IGBT\text{-}Water}$	ϑ_{Diode}	ϑ_{IGBT}
	W	W	°C	°C	°C	°C	°C
100% Diode	100	0	28	58	28	**123**	**93**
100% IGBT	0	100	28	28	41	**93**	**106**
⅔ IGBT ⅓ Diode	33	67	28	38	37	**103**	**102**

TABLE V
TEMPERATURE GRADIENTS AND JUNCTION TEMPERATURES AT $\vartheta_{Water} = 65$ °C (BEST SOLUTION—24 SCREWS WITH THERMAL-JOINT COMPOUND)

Losses sharing	$P_{Loss\text{-}Diode}$	$P_{Loss\text{-}IGBT}$	$\Delta\vartheta_{Case\text{-}Water}$	$\Delta\vartheta_{Diode\text{-}Water}$	$\Delta\vartheta_{IGBT\text{-}Water}$	ϑ_{Diode}	ϑ_{IGBT}
	W	W	°C	°C	°C	°C	°C
100% Diode	100	0	15	35	15	**100**	**80**
100% IGBT	0	100	15	15	28	**80**	**93**
⅔ IGBT ⅓ Diode	33	67	15	25	24	**90**	**89**

The results show that, under the assumed hypothesis, both the solutions with respect the junction-temperature limit (125 °C).

2) Temperatures Evaluation at Overload: In vehicle applications, the working profile of the traction drive is rather complex [26], and it is not deterministically defined as in the industrial applications [27]; the overload capability that is expected to be required by the application is in the range of 1.5× the nominal load for a few minutes.

The lumped-parameter steady-state model can be used to perform some evaluations about the overload capabilities of the IPMOT to be exploited in the real use.

The water temperature rising during the overload (higher losses in the motor and in the power converter) depends on the overall cooling circuit: In the considered solution (Fig. 1), it is estimated that the water temperature during the overload does not exceed 70 °C−75 °C.

Two overload situations are considered.

- Situation 1: 150% of the rated losses; in this case, it is assumed that, during the overload, the total drive losses bring the water temperature rising up to 70 °C.
- Situation 2: 200% of the rated losses; in this case, it is assumed that, during the overload, the total drive losses bring the water temperature rising up to 75 °C.

Both situations assume that 2/3 of the power losses are in the IGBT and 1/3 in the diode; the junction-temperature limit is fixed at 125 °C.

The situation 1 (150 W totally dissipated in each module—70-°C water temperature) is compatible even with the worst mounting solution (four screws without thermal-joint compound). The temperatures reported in Table VI basically respect the junction-temperature limit.

TABLE VI
TEMPERATURE GRADIENTS AND JUNCTION TEMPERATURES AT $\vartheta_{Water} = 70$ °C (WORST SOLUTION—FOUR SCREWS WITHOUT THERMAL-JOINT COMPOUND)

$P_{Loss\text{-}Diode}$		$P_{Loss\text{-}IGBT}$		$\Delta\vartheta_{Case\text{-}Water}$	$\Delta\vartheta_{Diode\text{-}Water}$	$\Delta\vartheta_{IGBT\text{-}Water}$	ϑ_{Diode}	ϑ_{IGBT}
%	W	%	W	°C	°C	°C	°C	°C
33	50	67	100	42	57	55	127	125

TABLE VII
TEMPERATURE GRADIENTS AND JUNCTION TEMPERATURES AT $\vartheta_{Water} = 75$ °C (BEST SOLUTION—24 SCREWS WITH THERMAL-JOINT COMPOUND)

$P_{Loss\text{-}Diode}$		$P_{Loss\text{-}IGBT}$		$\Delta\vartheta_{Case\text{-}Water}$	$\Delta\vartheta_{Diode\text{-}Water}$	$\Delta\vartheta_{IGBT\text{-}Water}$	ϑ_{Diode}	ϑ_{IGBT}
%	W	%	W	°C	°C	°C	°C	°C

TABLE VIII
IPMOT DRIVE RATINGS

4 phases Switched Reluctance Motor		
Nominal Power	24	kW
Nominal Torque	440	Nm
Base Speed	520	rpm
Constant Power Speed range	520-2600	rpm
Nominal phase current	75	A
DC link voltage	400	V

The situation 2 (200 W totally dissipated in each module—75-°C water temperature) is compatible only with the best mounting solution (24 screws with thermal-joint compound), as shown in Table VII.

In conclusion, under the assumed hypothesis, the module can stand twice the rated losses until the water temperature stays below 75 °C.

V. CONCLUSION

The cooling system of the power electronic converter of the IPMOT has been studied by means of a lumped-parameter steady-state model. The parameters have been evaluated by experimental tests and FEM simulation. A key problem is the thermal contact between the aluminum base plate and the steel motor housing; the contact depends on the quality of the surfaces, but the use of the thermal-joint compound and/or pressing together with "many" screws, the two parts dramatically reduce the contact thermal resistance. In any case, at rated load, the temperature of the power-electronic components does not exceed the limit.

Under reasonable assumptions and simplifications, the steady-state model shows useful overload margins, provided that the thermal resistance between the aluminum base plate and the steel motor housing has been minimized.

APPENDIX

See Table VIII.

ACKNOWLEDGMENT

The authors would like to thank the project coordinator Dr. H. Bendien (ITAPS) and Dr. M. Karas (ITAPS) for their valuable contribution, as well as P. Novotny (SKODA) for the machine prototyping.

REFERENCES

[1] S. Bauer, R. W. De Doncker, and D. Rossi, "Design of an integrated switched reluctance machine traction drive for an autonomous freight wagon," in *Proc. 21st Int. Elect. Vehicle Symp.*, Apr. 2005, CD-ROM.

[2] N. Mutoh, T. Kazama, and K. Takita, "Driving characteristics of an electric vehicle system with independently driven front and rear wheels," *IEEE Trans. Ind. Electron.*, vol. 53, no. 3, pp. 803–813, Jun. 2006.

[3] J. Moreno, M. E. Ortuzar, and J. W. Dixon, "Energy-management system for a hybrid electric vehicle, using ultracapacitors and neural networks," *IEEE Trans. Ind. Electron.*, vol. 53, no. 2, pp. 614–623, Apr. 2006.

[4] C. H. Chen and M. Y. Cheng, "Implementation of a highly reliable hybrid electric scooter drive," *IEEE Trans. Ind. Electron.*, vol. 54, no. 5, pp. 2462–2473, Oct. 2007.

[5] K. M. Rahman, B. Fahimi, G. Suresh, A. V. Rajarathnam, and M. Ehsani, "Advantages of switched reluctance motor applications to EV and HEV: Design and control issues," *IEEE Trans. Ind. Appl.*, vol. 36, no. 1, pp. 111–121, Jan./Feb. 2000.

[6] S. S. Ramamurthy and J. C. Balda, "Sizing a switched reluctance motor for electric vehicles," *IEEE Trans. Ind. Appl.*, vol. 37, no. 5, pp. 1256–1264, Sep./Oct. 2001.

[7] K. M. Rahman and S. E. Schulz, "Design of high-efficiency and high-torque-density switched reluctance motor for vehicle propulsion," *IEEE Trans. Ind. Appl.*, vol. 38, no. 6, pp. 1500–1507, Nov./Dec. 2002.

[8] S. Bauer, F. Farina, F. Profumo, D. Rossi, and A. Tenconi, "Thermal design of integrated motor drives for traction applications," in *Proc. EPE*, Sep. 2005, CD-ROM.

[9] M. Ehsani, K. M. Rahman, M. D. Bellar, and A. J. Severinsky, "Evaluation of soft switching for EV and HEV motor drives," *IEEE Trans. Ind. Electron.*, vol. 48, no. 1, pp. 82–90, Feb. 2001.

[10] R. Inderka, M. Menne, and R. De Doncker, "Control of switched reluctance drives for electric vehicle applications," *IEEE Trans. Ind. Electron.*, vol. 49, no. 1, pp. 48–53, Feb. 2002.

[11] S. Williamson and D. C. Jackson, "Integrated drives for industrial applications," in *Proc. PCIM*, Jun. 1999, pp. 9–13.

[12] R. J. Kerkman, G. L. Skibinski, and D. W. Schlegel, "AC drives: Year 2000 (Y2K) and beyond," in *Proc. IEEE APEC*, Mar. 1999, vol. 1, pp. 28–29.

[13] Y. Shakweh, G. H. Owen, D. J. Hall, and H. Miller, "Plug and play integrated motor drives," in *Proc. IEE Power Electron., Mach. Drives*, Jun. 2002, pp. 655–661.

[14] J. Rannenberg, Y. Tadros, and U. Schaefer, "Motor-integrated circular converter for hybrid electric vehicles," *EPE J.*, vol. 14, no. 2, pp. 23–27, Mar.–May 2004.

[15] C. Klumpner, F. Blaabjerg, and P. Thoegersen, "Alternate ASDs: Evaluation of the converter topologies suited for integrated motor drives," *IEEE Ind. Appl. Mag.*, vol. 12, no. 2, pp. 71–83, Mar./Apr. 2006.

[16] P. W. Wheeler, K. J. Bradley, S. Pickering, and F. Thovex, "Thermal design of an integrated motor drive," in *Proc. IEEE IECON*, Nov. 2006, pp. 4794–4799.

[17] N. R. Brown, T. M. Jahns, and R. D. Lorenz, "Power converter design for an integrated modular motor drive," in *Conf. Rec. IEEE IAS Annu. Meeting*, Sep. 2007, pp. 1322–1328.

[18] P. N. Materu and R. Krishnan, "Estimation of switched reluctance motor losses," *IEEE Trans. Ind. Appl.*, vol. 28, no. 3, pp. 668–679, May/Jun. 1992.

[19] I. Chindurza, D. G. Dorrell, and C. Cossar, "Assessing the core losses in switched reluctance machines," *IEEE Trans. Magn.*, vol. 41, no. 10, pp. 3907–3909, Oct. 2005.

[20] D. Staton, A. Boglietti, and A. Cavagnino, "Solving the more difficult aspects of electric motor thermal analysis in small and medium size industrial induction motors," *IEEE Trans. Energy Convers.*, vol. 20, no. 3, pp. 620–628, Sep. 2005.

[21] J. Driesen, R. J. M. Belmans, and K. Hameyer, "Finite-element modeling of thermal contact resistances and insulation layers in electrical machines," *IEEE Trans. Ind. Appl.*, vol. 37, no. 1, pp. 15–20, Jan./Feb. 2001.

[22] R. Inderka, C. Carstensen, and R. De Doncker, "Eddy currents in medium power switched reluctance machines," in *Proc. IEEE PESC*, Jun. 2002, vol. 2, pp. 979–984.

[23] M. Klauz and D. G. Dorrell, "Eddy current effects in a switched reluctance motor," *IEEE Trans. Magn.*, vol. 42, no. 10, pp. 3437–3439, Oct. 2006.

[24] H. A. Mantooth and A. R. Hefner, Jr., "Electrothermal simulation of an IGBT PWM inverter," *IEEE Trans. Power Electron.*, vol. 12, no. 3, pp. 474–484, May 1997.

[25] D. Xu, H. Lu, L. Huang, S. Azuma, M. Kimata, and R. Uchida, "Power loss and junction temperature analysis of power semiconductor devices," *IEEE Trans. Ind. Appl.*, vol. 38, no. 5, pp. 1426–1431, Sep./Oct. 2002.

[26] M. A. Valenzuela, P. V. Verbakel, and J. A. Rooks, "Thermal evaluation for applying TEFC induction motors on short-time and intermittent duty cycles," *IEEE Trans. Ind. Appl.*, vol. 39, no. 1, pp. 45–52, Jan./Feb. 2003.

[27] M. Ehsani, K. M. Rahman, and H. A. Toliyat, "Propulsion system design of electric and hybrid vehicles," *IEEE Trans. Ind. Electron.*, vol. 44, no. 1, pp. 19–27, Feb. 1997.

Alberto Tenconi (M'99) received the M.Sc. and Ph.D. degrees in electrical engineering from the Politecnico di Torino, Turin, Italy, in 1986 and 1990, respectively.

From 1988 to 1993, he was with the Electronic System Division, FIAT Research Center, Turin, where he was engaged in the development of electric-vehicle drive systems. He is currently a Professor of electrical machines with the Dipartimento di Ingegneria Elettrica, Politecnico di Torino. His fields of interest are high-performance drive design, new power-electronic device applications, and nonconventional electric-machine development. His research activity is documented by more than 120 papers published in international journals and conference proceedings. He has participated, both as designer and as scientific responsible, in many national and European research programs. He is also a Reviewer for international journals.

Francesco Profumo (M'88–SM'90) was born in Savona, Italy, in 1953. He received the M.Sc. degree in electrical engineering from the Politecnico di Torino, Turin, Italy, in 1977.

From 1978 to 1984, he was a Senior Engineer with the R&D Ansaldo Group, Genoa, Italy. From 1984 to 1995, he was an Associate Professor with the Dipartimento di Ingegneria Elettrica, Politecnico di Torino, where he is currently a Professor of electrical machines and drives and a Rector. He was a Visiting Professor in the Department of Electrical and Computer Engineering, University of Wisconsin, Madison, from 1986 to 1988 and in the Department of Electrical Engineering and Computer Science, Nagasaki University, Nagasaki, Japan, for one semester from 1996 to 1997. His fields of interest are power-electronic conversion, high-power devices, applications of new power devices, integrated electronic/electromechanical design, high-response-speed servo drives, and new electrical-machine structures. He has published more than 200 papers in international conference proceedings and technical journals.

Prof. Profumo is a member of the technical program committees of several international conferences in the power-electronic and motor-drive fields. He was the Technical Cochairman of PCC'02 in Osaka, Japan, in 2002. He has been the coordinator or partner of several projects in the frame of European Commission activities. He is a Registered Professional Engineer in Italy.

Stefan E. Bauer received the Diploma degree in electrical engineering from RWTH Aachen University, Aachen, Germany, in 1999.

In March 2001, he was a Research Associate with the Institute for Power Electronics and Electrical Drives, RWTH Aachen University. His research activities are in the area of switched reluctance drives and their controls. In 2007, he founded the company Durotron, Cologne, Germany. The company focuses on custom-made electrical drives and control solutions.

Martin D. Hennen (M'06) was born in Saarburg, Germany, in 1980. He received the Diploma degree in electrical engineering from RWTH Aachen University, Aachen, Germany, in 2005.

Since November 2005, he has been a Research Associate with the Institute for Power Electronics and Electrical Drives, RWTH Aachen University. His main interests are in the field of switched reluctance drives and their controls.